Article

Size-resolved identification, characterization and quantification of primary biological organic aerosol at a European rural site

Carlo Bozzetti, Kaspar R Daellenbach, Christoph Hueglin, Paola Fermo, Jean Sciare, Anneliese Kasper-Giebl, Yinon Mazar, Guelcin Abbaszade, Mario El Kazzi, Raquel Gonzalez, Timor Shuster-Meiseles, Mira Flasch, Robert Wolf, Adela Krepelova, Francesco Canonaco, Jürgen Schnelle-Kreis, Jay G. Slowik, Ralf Zimmermann, Yinon Rudich, Urs Baltensperger, Imad El Haddad, and Andre S.H. Prevot

Environ. Sci. Technol., **Just Accepted Manuscript** • DOI: 10.1021/acs.est.5b05960 • Publication Date (Web): 22 Feb 2016

Size-resolved identification, characterization and quantification of primary biological organic aerosol at a European rural site

Carlo Bozzetti[†], Kaspar R. Daellenbach[†], Christoph Hueglin[‡], Paola Fermo[≠], Jean Sciare[r], Anneliese Kasper-Giebl[ǒ], Yinon Mazar[•], Gülcin Abbaszade[¯], Mario El Kazzi[¤], Raquel Gonzalez[≠], Timor Shuster-Meiseles[•], Mira Flasch[ǒ], Robert Wolf[†], Adéla Křepelová[†], Francesco Canonaco[†],Jurgen Schnelle-Kreis[¯], Jay G. Slowik[†], Ralf Zimmermann[¯,◊], Yinon Rudich[•], Urs Baltensperger[†], Imad El Haddad[†], and André S. H. Prévôt[†*]*

† Laboratory of Atmospheric Chemistry, Paul Scherrer Institute, Villigen 5232, Switzerland

‡ Swiss Federal Laboratories for Materials Science and Technology, EMPA, Dübendorf 8600, Switzerland

≠ Università degli Studi di Milano, Milano 20133, Italy

r Laboratoire des Sciences du Climat et de l'Environnement, LSCE, CNRS-CEA-UVSQ, Gif-sur-Yvette 91190, France

ǒ Institute of Chemical Technologies and Analytics, Vienna University of Technology, Wien 1060, Austria

• Department of Earth and Planetary Sciences, Weizmann Institute of Science, Rehovot 76100, Israel

19 ⊐ Helmholtz Zentrum München, German Research Center for Environmental Health (GmbH),
20 Joint Mass Spectrometry Centre, Cooperation Group Comprehensive Molecular Analytics,
21 85764 Neuherberg, Germany

22 ¤ Electrochemistry Laboratory, Paul Scherrer Institute, Villigen 5232, Switzerland

23 ◊ Analytical Chemistry & Joint Mass Spectrometry Centre, Institute of Chemistry, University of
24 Rostock, 18051 Rostock, Germany

25 E-mail: imad.el-haddad@psi.ch, andre.prevot@psi.ch

26 **Abstract**

27 Primary biological organic aerosols (PBOA) represent a major component of the coarse
28 organic matter (OM_{COARSE}, aerodynamic diameter >2.5μm). Although this fraction affects
29 human health and climate, its quantification and chemical characterization currently remain
30 elusive. We present the first quantification of the entire $PBOA_{COARSE}$ mass and its main sources
31 by analyzing size-segregated filter samples collected during summer and winter at the rural site
32 of Payerne (Switzerland), representing a continental Europe background environment. The size-
33 segregated water soluble OM was analyzed by a newly developed offline aerosol mass
34 spectrometric technique (AMS). Collected spectra were analyzed by 3-dimensional positive
35 matrix factorization (3D-PMF), showing that PBOA represented the main OM_{COARSE} source
36 during summer and its contribution to PM_{10} was comparable to that of secondary organic
37 aerosol. We found substantial cellulose contributions to OM_{COARSE}, which in combination with
38 gas chromatography mass spectrometry molecular markers quantification, underlined the
39 predominance of plant debris. Quantitative polymerase chain reaction (qPCR) analysis instead

revealed that the sum of bacterial and fungal spores mass represented only a minor OM_{COARSE} fraction (<0.1%). X-ray photoelectron spectroscopic (XPS) analysis of C and N binding energies throughout the size fractions revealed an organic N increase in the PM_{10} compared to PM_1 consistent with AMS observations.

Introduction

Primary biological organic aerosol (PBOA) is a major source of coarse aerosol organic matter (OM). The detection of these particles has been the subject of studies for one and a half centuries.[1-3] Studies[4] have related single PBOA components to adverse health effects,[5] and revealed their important role as ice and cloud condensation nuclei.[6-10] Emissions of primary biological particles (PBAP) are estimated to be among the largest contributors of pre-industrial organic aerosols,[11] therefore a precise estimate of their sources is also important for the development of accurate climate models.[4] Nevertheless, PBOA characterization and quantification has received less attention than other types of aerosol sources and processes (e.g. traffic, mineral dust, sulfate, wood combustion and secondary organic aerosol), possibly because of technical limitations hindering the understanding of the sources and composition of this fraction.

Traditional analytical techniques for the PBOA characterization include optical microscopy, cultivation of specific viable bacteria, fungi and algae and fluorescence microscopy for the quantification of functionalized or autoflorescent specific components.[4] More recent approaches are classified into molecular techniques (e.g. chemical tracers determination, nucleic acids extraction and amplification), optical techniques (fluorescent and Raman spectroscopy), and non-optical techniques. Fluorescence techniques are of particular relevance because biological

materials contain fluorophores.[12,13] Non-optical approaches include different types of mass spectrometers; among these, we note the recent use of online-aerosol mass spectrometry (AMS) for the study of the submicron fraction.[14-16]

Despite the vast literature focusing on the quantification of individual PBOA components, the quantification of the total PBOA mass and the main processes by which this fraction enters the atmosphere remains elusive. As a consequence, the International Panel on Climate Change 2013[17] reported the global terrestrial PBOA emission to range between 50 and 1000 Tg/yr, highlighting the large gap in our knowledge about this fraction. Within this fraction, 28 Tg/yr were estimated to comprise fungal spore emissions using arabitol and mannitol as tracers.[18] The use of these compounds as specific fungal spores tracers is still subject of discussion in the scientific community[19,20] and there is a general indispensable need for the determination of PBOA concentrations and major emission processes through size-resolved field observations against which the global models can be evaluated.

In this study, we present the first quantification of the total water-soluble PBOA (WSPBOA) mass using an offline Aerodyne Time-of-Flight Aerosol Mass Spectrometer (ToF-AMS). The analysis was performed on PM_1, $PM_{2.5}$ and PM_{10} (particulate matter with an aerodynamic diameter < 1, 2.5 and 10 μm) filter samples collected concomitantly at the rural site of Payerne, Switzerland. WSPBOA quantification was achieved by 3-dimensional positive matrix factorization analysis (3D-PMF) of water soluble OA mass spectra, following the recently developed methodology described by Daellenbach.[21] In comparison with previous PBOA online AMS observations,[14-16] the filter samples water extraction step enabled accessing the $WSOM_{COARSE}$ fraction. For the characterization of the main PBOA sources, the dataset was complemented with an unprecedented combination of measurements, including enzymatic

cellulose determination, quantification of bacterial and fungal spore DNA via quantitative polymerase chain reaction (qPCR), and gas chromatography mass spectrometry analysis (GC-MS) of organic molecular markers. In this study, we discuss the quantification of the total PBOA mass via 3D-PMF, the quantification of its major components and their possible usage as PBOA tracers including bacteria and fungal spores measured via qPCR, plant debris estimate from *n*-alkanes measurements, and carbohydrates.

Material and Methods

Sample collection. We collected in total 87 24h-integrated aerosol samples (Batch A) on quartz fiber filters at the rural background site of Payerne during June-July 2012 and January-February 2013. Batch A included PM_1, $PM_{2.5}$, and PM_{10} samples collected in parallel using three High-Volume samplers (Digitel DA-80H equipped with PM_1, $PM_{2.5}$ and PM_{10} size-selective inlets) operating at 500 L min^{-1}. In total 45 samples were collected during summer (15 samples per size fraction), and 42 during winter (14 samples per size fraction). Additionally, PM_{10} filters were collected every fourth day throughout 2013 following the same procedure (Batch B). In the following, the subscript *coarse* will denote for a generic aerosol component, the fraction contained between 2.5 and 10 μm.

Aerosol characterization. An overview of the auxiliary analytical measurements can be found in Table 1, Table S2, and in the Supplementary Information (SI). In this section only offline-AMS, qPCR, and x-ray photoelectron spectroscopy (XPS) will be discussed in details.

Table 1. Supporting measurements

Measured variable	Batch A	Batch B

PM	Gravimetry	All filters	-
WSOM mass spectral fingerprint	Offline-AMS[21]	All filters	All filters
EC/OC	Thermal Optical Transmittance using a Sunset Lab Analyzer[22] (EUSAAR2)[23]	All filters	-
ions	Ion Chromatography[24]	All filters	-
WSOC	Water extraction Thermal Decomposition ND-IR determination using TOC analyzer (SI)	All filters	-
Cellulose	Cellulose enzymatic conversion to D-glucose and photometric determination[25]	32 filters (9 summer PM_{10} filters, 4 winter PM_{10}, 5 summer $PM_{2.5}$, 9 summer PM_1, and 5 summer PM_1)	-
molecular markers (Table S2)	In-Situ Derivatization Thermal Desorption Gas Chromatography Time-of-Flight Mass Spectrometry (IDTD-GC-MS)[26]	40 samples (15 summer PM_1, 15 summer PM_{10}, 5 winter PM_1, 5 winter PM_{10})	-
C1s, N1s Binding energies	X-Ray Photoelectron Spectroscopy	6 samples (3 summer PM_{10}, 3 summer PM_1)	-
bacterial and fungal spore DNA	Quantitative Polymerase Chain Reaction genetic analysis[27,28]	58 samples (all summer PM_1, $PM_{2.5}$, and PM_{10}, all winter PM_1 and PM_{10})	-
Carbohydrates (Table S2)	IC coupled to a Pulsed Amperometric Detector (IC-PAD)[29]	All samples	-

Offline-AMS. The Offline-AMS analysis entails an extraction of two 16 mm diameter punches per sample in 10 mL of ultrapure water (18.2 MΩcm, Total Organic Carbon < 5 ppb) via ultra-sonication for 20 min at 30°C. Liquid extracts were subsequently homogenized for 40 s using a

vortex mixer and then filtered through 0.45 μm nylon membrane syringe filters. Filtered extracts were aerosolized and the generated particles were dried using a silica gel diffusion drier before measurement by HR-ToF-AMS.[30] On average 10 mass spectra (60 s each) of the bulk WSOM were collected per extract. Before each sample measurement, 5 blank mass spectra were collected by nebulizing ultrapure water, and their average was subtracted from the corresponding individual sample mass spectra. The signal of field blank samples measured following the same procedure was statistically not different from the ultrapure water mass spectra.

XPS. XPS analysis enabled monitoring the binding energies (BE) of C, S and N, providing insight into their oxidation state (typically higher BE are related to higher oxidation numbers), and thereby quantifying the organic N (N_{org}) mass through the size fractions. The same analysis was conducted on 3 field blanks and on N-containing surrogate standards deposited on blank quartz fiber filters. Tested standards included $NaNO_3$ and $(NH_4)_2SO_4$ for the characterization of the most abundant forms of inorganic N, while horseradish peroxidase and chloroperoxidase from *caldariomyces fumago* were used as surrogates for amine and amide containing proteins in PBOA. Signal identification and integration proceeded as follows. The obtained spectra were first aligned with a two-point BE calibration using the Si_{2p} and the O_{1s} peaks deriving from the quartz fiber filters as reference points. We estimated an energy accuracy of 0.3 eV, and an average fitting error of 1.4% by fitting the signals of replicate measurements of standard compounds and blanks and assuming a single Gaussian peak for each atom. These parameters were then used for the fitting of the blank-subtracted C_{1s}, and N_{1s} signals in environmental samples, which consisted of several peaks from different chemical components. The number of these peaks was determined such that fitting residuals (fraction of signal) equaled the fitting errors determined from the fitting of single compounds. The N_{1s} peak widths were constrained to

be equal to the one derived from $(NH_4)_2SO_4$ standard, while the C_{1s} peak width was determined from blank filters. From the analysis of standard $(NH_4)_2SO_4$ we derived an average N_{1s}/S_{2p} ratio of 0.80±0.02, which was used to estimate the N_{1s} contribution from $(NH_4)_2SO_4$ ($N_{1s(NH_4)_2SO_4}$). This contribution was fixed in proportion of that of S_{2p} using the aforementioned N_{1s}/S_{2p} ratio and N_{1s} peak width. This estimate neglected the contribution from organic or non-$(NH_4)_2SO_4$ sulfate. The uncertainty on the $N_{1s(NH_4)_2SO_4}$ area was estimated based on the integration of the S_{2p} peak. N_{1s} fitting sensitivity analysis was performed by varying the $N_{1s(NH_4)_2SO_4}$ peak position and area within our uncertainties. Only fittings of $N_{1s(NH_4)_2SO_4}$with residuals lower than our errors were retained.

qPCR. We performed a qPCR analysis in order to quantify total bacterial and fungal spore DNA. DNA extraction was conducted following the procedure presented in the SI and specific universal primers (Table S3) were selected for total DNA quantification of bacterial and fungal spores. The extracted DNA was amplified using the qPCR technique described in Lang-Yona.[27,28] The total number of bacterial cells and fungal spores was estimated assuming a DNA content of $4.74 \cdot 10^{-3}$ pg per bacterial cell and $3 \cdot 10^{-2}$ pg per fungal spore respectively, based on the *Escherichia coli* and *Aspergillus fumigatus* genome lengths (4,639,221 bp and 29,384,958 bp, respectively).[31] Total bacterial mass was estimated for PM_1 and PM_{10} samples assuming as a reference the dry and wet *E. coli* cell weights ($3 \cdot 10^{-13}$ and $1 \cdot 10^{-12}$ g, respectively),[32] while total fungal spores mass was based on the *A. fumigatus* spore weight of $2.9 \cdot 10^{-12}$ g.[33]

3D-PMF

OA mass spectra collected by offline-AMS were analyzed using 3D-PMF to apportion the time-dependent size-segregated (PM_1, $PM_{2.5}$, PM_{10}) contributions of the water soluble organic

sources.[34] We adopted a vector-matrix approach,[35] also known as "Tucker1" approach[36] in which we assumed constant mass spectra throughout the size fractions. The 3D-PMF algorithm describes the variability of the multivariate data-matrix (x) as the linear combination of static factor profiles (f) and their corresponding time and size-dependent contributions (g), such that

$$x_{i,j,k} = \sum_{z=1}^{p} g_{i,j,z} \cdot f_{z,k} + e_{i,j,k} \quad (1)$$

Here, $x_{i,j,k}$ denotes an element of the data matrix, while subscripts i, j and k represent time, size and organic ions (250 fitted organic ions in the range m/z 12 to 115) respectively. The subscripts p and z indicate the total number of factors selected by the user, and a discrete factor number ($1 \leq z \leq p$) respectively, while $e_{i,j,k}$ represents an element of the residual matrix.

PMF was solved using the multi-linear engine algorithm (ME-2)[37,38] (using the source finder, SoFi)[38] which enabled an efficient exploration of the rotational ambiguity by directing the solution toward environmentally relevant rotations. This was achieved by a-priori constraining $f_{z,k}$ and/or $g_{i,j,z}$ elements, and allowing the constrained elements to vary within a predetermined range defined by a scalar a, such that the returned $f_{z,k}'$ or $g_{i,j,z}'$ values satisfy eq 2.

$$f_{z,k}' = f_{z,k} \pm a \cdot f_{z,k} \quad (2)$$

Here we constrained the f matrix elements for only one factor, related to hydrocarbon-like organic aerosol (HOA) from traffic[39] (SI).

PMF data and error input matrices (x and s) were constructed including ten mass spectral repetitions per filter sample. Data and error matrices were rescaled to $WSOM_i$ in order to compare source apportionment results with external tracers. $WSOM_i$ concentrations were estimated from the $WSOC_i$ measurements multiplied by the OM/OC_i ratios determined from offline-AMS HR analysis (measured OM/OC_i distribution 1st quartile 1.89, 3rd quartile 2.01).[40] In

178 total, the 3D-PMF input matrices comprised 87 samples corresponding to 29 filters per size
179 fractions.
180 The error matrix elements $s_{i,j,k}$ were determined according to eq 3 by propagating the blank
181 standard deviation $\sigma_{i,j,k}$ and the signal error $\delta_{i,j,k}$ accounting for electronic noise, ion-to-ion
182 variability at the detector, and ion counting statistics.[41,42]

183 $$s_{i,j,k} = \sqrt{\delta_{i,j,k}^2 + \sigma_{i,j,k}^2} \quad (3)$$

184 The optimization of the 3D-PMF results is thoroughly presented in the SI. Briefly, to improve
185 the factor separation we up-weighted selected variables dividing their corresponding
186 uncertainties by a scalar *c* (>1).[43] The sensitivity of model outputs to *c* and *a*-values was assessed
187 and only solutions matching selected criteria were retained (SI). The variability of the results
188 amongst the selected solutions was considered our best estimate of model errors.
189 PMF factor contributions to total OM were estimated after PMF analysis as:

190 $$ZOA_i = \frac{WSZOA_i}{R_z} \quad (4)$$

191 Here, [*WSZOA*] and [*ZOA*] denote for a generic *Z* source the concentration of the ambient water
192 soluble organic aerosol and the total organic aerosol respectively, while R_z indicates the recovery
193 efficiency for that source. In total, 5 OA factors were separated including HOA, summer
194 oxygenated OA (S-OOA), winter oxygenated OA (W-OOA), biomass burning OA (BBOA), and
195 primary biological OA (PBOA). The $R_{z,med}$ determined by Daellenbach[21] were applied to all
196 factors except for PBOA, whose recovery was not previously estimated. Accordingly, we shall
197 report hereafter the concentration of WSPBOA and estimate the PBOA water solubility.
198 Source apportionment errors ($\sigma_{S.A.,Z,i}$) were estimated according to eq 5, which accounts for R_Z
199 and rotational uncertainty ($\sigma_{PMF,RZ,i}$), measurement repeatability ($\sigma_{REP,i}$), and WSOM uncertainty
200 ($\sigma_{WSOC,i}$).

$$\sigma_{S.A.,Z,i} = \sqrt{\sigma^2_{PMF,RZ,i} + \sigma^2_{REP,Z,i} + f^2_{Z,i} \cdot \sigma^2_{WSOM,i}} \quad (5)$$

Here f_Z denotes the relative contribution of the generic factor Z to WSOM. $\sigma_{WSOM,i}$ includes WSOC blank variability and measurement repeatability. The $\sigma_{PMF,RZ,i}$ term includes the variability of the rescaled PMF solutions and represents our best estimate of recovery errors and rotational ambiguity. The $\sigma_{REP,Z,i}$ term was considered as our best estimate of experimental repeatability/errors and represents the variability of PMF results for the measurements repetitions.

Results and Discussion

PM major components

A complete overview of the size-segregated chemical composition of winter and summer PM components is presented in Figure 1a. In the following, average and median values are indicated with the subscripts *avg* and *med*, respectively.

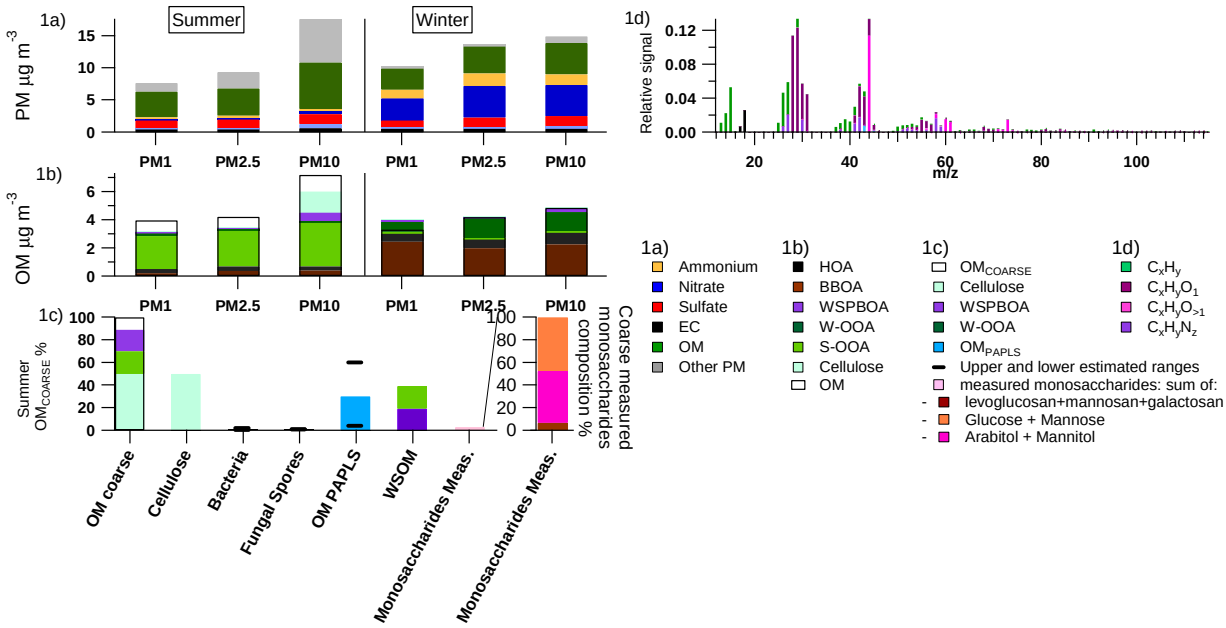

Figure 1. 1a) Seasonal PM chemical composition of the different size fractions. The OM_i estimate was calculated from OC_i measurements multiplied by the corresponding OM/OC_i retrieved from offline-AMS HR analysis. 1b) Average seasonal aerosol sources contributions to OM in the different size fractions. White are consistent with our estimate of the water insoluble PBOA fractions (Figure S8). 1c) Summer OM_{COARSE} major components. 1d) WSPBOA high resolution AMS mass spectrum.

OM represented a major component of PM during summer and winter. While during winter large part of the OM_{10} (87%) was comprised in the $PM_{2.5}$ fraction, during summer this fraction represented only 58%. In contrast, during summer secondary inorganic species (SO_4^{2-}, NH_4^+, and NO_3^-) did not manifest a comparable increase in PM_{COARSE} (85% of the mass comprised in the $PM_{2.5}$ fraction) suggesting a small contribution of additional secondary aerosols in the coarse fraction. Overall OM_{COARSE} accounted for 3 μg m^{-3}_{avg} during summer, and as will be shown in the following, large part of this fraction constituted of PBOA (Figure S13).

Similarly to OM, dust likely from resuspension[44] was enhanced in the coarse fraction especially during summer. The upper limit for the inorganic $dust_{COARSE}$ concentration was estimated as the difference between inorganic PM_{10} and inorganic $PM_{2.5}$ ($PM_{COARSE,inorg}$), and accounted for 31%$_{avg}$ during summer and 5%$_{avg}$ during winter, although this estimate can include small sea salt contributions (SI). The obtained $(Ca^{2+}/PM)_{COARSE,inorg}$ value of 4.2%$_{med}$ (1st quartile 3.2%, 3rd quartile 7.7%) was consistent with the ratios reported by Chow[45] for 20 different dust profiles (3.5±0.5%), and with values reported by Amato in Zürich.[46] As a comparison, the total OM_{COARSE} concentration represented 36%$_{avg}$ of PM_{COARSE} (8.4 μg m^{-3}), compared to the 62%$_{avg}$ for $dust_{COARSE,inorg}$.

Size resolved OA source apportionment

In this section we present the validation of the 3D-PMF factors (HOA, BBOA, W-OOA, S-OOA, and WSPBOA) which enabled the quantification of WSPBOA. Average source apportionment results are presented in Figure 1b and Figure 2.

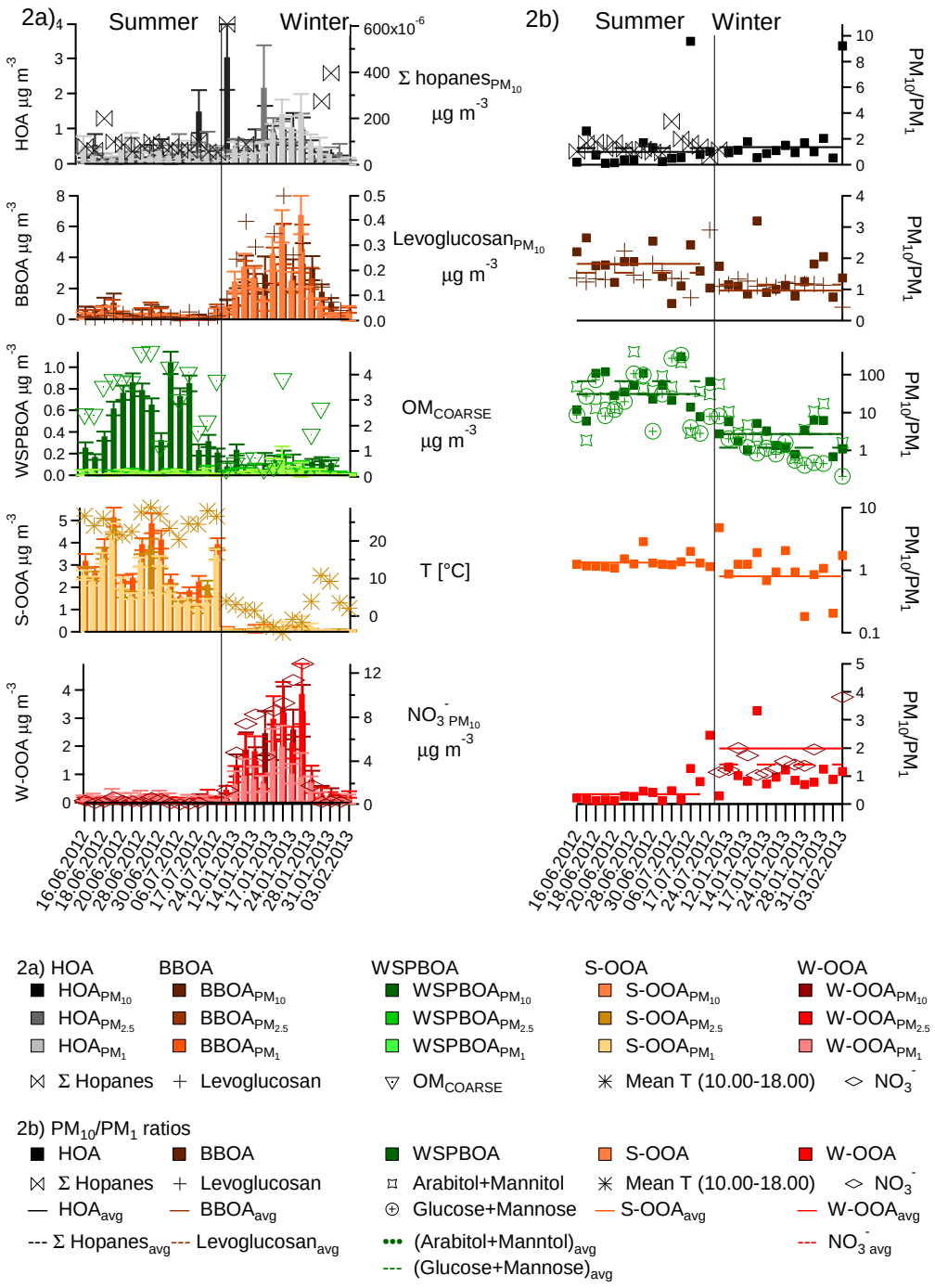

Figure 2. 3D-PMF source apportionment results. 2a) Size fractional time series of PMF factors, corresponding tracers, and temperature. Error bars represent source apportionment uncertainty. 2b) Size fractional increase (PM_{10}/PM_1) time series of PMF factors, and corresponding tracers.

3D-PMF factors were associated to aerosol sources or processes according to mass spectral features, seasonal contributions, size fractional contributions, and correlation with tracers (Figure 2). Given the lack of widely accepted methodologies to estimate the uncertainty of PMF results, in this work we considered $\sigma_{S.A.,k,i}$ (Methodology section) as our source apportionment uncertainty, while the statistical significance of the factor contributions for each size fraction was based on our best error estimation ($\sigma_{S.A.,k,i}$, Table S4).

HOA and BBOA contributions represented the only anthropogenic primary sources resolved in Payerne. In particular, HOA correlated with hopanes present in lubricant oils with a R=0.54 (SI). This correlation is also supported by the summer $(HOA/EC)_{med}$ ratio (0.63_{med}) being consistent with other European studies reported by El Haddad and references therein.[47] BBOA instead correlated with levoglucosan produced by cellulose pyrolysis (R=0.94). A levoglucosan/BBOC ratio of 0.18_{med} was found, consistent with values reported (Huang and references therein[48]) for ambient BBOA observations. Both HOA and BBOA showed statistically significant contributions (>3σ) only in the submicron fractions. The seasonal trend of these anthropogenic factors was also significantly different: while the HOA (traffic) contribution was relatively stable and small across the year, BBOA showed a strong seasonality, rising from $6\%_{avg}$ of OM_1 during summer to $73\%_{avg}$ during winter.

Two OOA factors characterized by high CO_2^+ contributions were separated according to their different seasonal trends. While W-OOA showed a strong correlation with NO_3^- (R=0.94), S-OOA showed a positive non-linear correlation with temperature, following the behavior of biogenic volatile organic compounds emissions.[49] The relative contribution of W-OOA to OM_1

rose from 5%$_{avg}$ during summer to 22%$_{avg}$ during winter, while the S-OOA contribution to OM_1 decreased from 59%$_{avg}$ during summer to 4%$_{avg}$ during winter. W-OOA was the only factor significantly contributing (within 3σ) to OM in the size range 1-2.5 μm (48%$_{avg}$ of the W-OOA mass in winter), while the $W\text{-}OOA_{COARSE}$ contribution was never statistically significant. NH_4NO_3 behaved similarly with 31%$_{avg}$ of the mass in winter comprised in $PM_{2.5}$-PM_1. During summer instead S-OOA showed a different behavior in the three size fractions: its contribution was significant for PM_1, but not in the size range 1-2.5 μm. The overall $S\text{-}OOA_{2.5}$ fraction accounted for 82±2%$_{avg}$ of the mass, while the remaining 18±2%$_{avg}$ was included in OM_{COARSE}. Considering the sum of both OOA factors, the $OOA/NH_4^+{}_{med}$ ratio for PM_1 was 2.1, consistent with values reported by Crippa[50] for 25 different European rural stations, suggesting that Payerne can be representative of typical European rural environments.

The last PMF factor showed an unusual size fractionation with 96%$_{avg}$ of its mass comprised in the PM_{COARSE} during summer (0.54±0.02 μg m^{-3}), corresponding to 49% of the $WSOM_{COARSE}$ (or 19%$_{avg}$ of the OM_{COARSE}). This factor was ascribed to water soluble primary biological organic aerosol, given its striking mass spectral resemblance to biological carbohydrates and plant debris extracts with high contribution from $C_2H_4O_2^+$, $C_2H_5O_2^+$ and $C_3H_5O_2^+$ (Figure 1d, S3, S10), its enhancement in OM_{COARSE} especially during summer, and its correlations with biological aerosol components such as arabitol, mannitol, glucose,[19,20,51,52] cellulose, total bacteria, and fungal spores. The detection of such factor was unprecedented in the AMS literature given the limited transmission efficiency of the AMS aerodynamic lens for the coarse fraction,[53] although Schneider[15] proposed the use of some of the PBOA fragments detected here to assess the contribution of PBOA to PM_1 from online AMS measurements in the Amazon.

Also during winter WSPBOA showed a smaller but still significant contribution to the OM_{COARSE} (30% of $WSOM_{COARSE}$ or 8% of OM_{COARSE}) with $68\%_{avg}$ of the mass comprised in the coarse fraction. This result was corroborated by a minor but statistically significant enhancement in the coarse fraction (in comparison with $PM_{2.5}$) of biological carbohydrates ($monosaccharides_{BIO}$: Σ(glucose, mannose, arabitol and mannitol)), cellulose, and fungal spores. The chemical characteristics and origin of this fraction will be thoroughly discussed in the following sections.

Composition of OM_{COARSE}.

This section presents a detailed characterization of OM_{COARSE}, of which $91\%_{avg}$ of the mass was ascribed to PBOA.

Water soluble and insoluble OM_{COARSE}. Figure 1c displays the relative chemical composition of OM_{COARSE} during summer. The major part of OM_{COARSE} could be ascribed to cellulose ($50\pm20\%_{avg}$) and $WSOM_{COARSE}$ ($38\%_{avg}$). Given the low cellulose water solubility, and consequently its negligible contribution to WSOM, the two fractions together accounted for $88\%_{avg}$ of the OM_{COARSE}. Regarding the origin of the $WSOM_{COARSE}$ fraction, 3D-PMF results revealed that only WSPBOA and WSS-OOA contributed significantly to $WSOM_{COARSE}$ during summer, explaining respectively $51\%_{avg}$ and $49\%_{avg}$ of the $WSOM_{COARSE}$ mass. Assuming the water insoluble OM_{COARSE} fraction not ascribed to S-OOA to be entirely related to PBOA, we calculated a R_{PBOA} lowest estimate of 0.18_{med} (1^{st} quartile 0.15, 3^{rd} quartile 0.25) according to eq S2, S3 and S4. This assumption was corroborated by the high cellulose contributions to the water insoluble OM_{COARSE} fraction ($82\%_{avg}$) and by the good correlation of WSPBOA with OM_{COARSE}-$S\text{-}OOA_{COARSE}$ (R=0.54), especially considering that the water insoluble OM_{COARSE} fraction represented $62\%_{avg}$ of the total OM_{COARSE}.

Contribution of carbohydrates to PBOA and OM_{COARSE}. Measured carbohydrates ($carbohydrates_{meas}$: Σ ($monosaccharides_{BIO}$, mannosan, levoglucosan, and galactosan)) represented 3% of OM_{COARSE} (8% of $WSOM_{COARSE}$), of which $93\%_{avg}$ was related to $monosaccharides_{BIO}$. This fraction, albeit minor, was highly correlated with PBOA (R=0.73) and cellulose (R=0.85), showing a size fractionation similar to WSPBOA especially during summer with $96\%_{avg}$ of the mass included in the OM_{COARSE}. A similar behavior was noted in winter, with $29\%_{avg}$ of the $carbohydrates_{meas,COARSE}$ consisting of $monosaccharides_{BIO}$, suggesting a minor, but statistically significant contribution of primary biological emissions, consistent with WSPBOA from 3D-PMF results (figure 2). Also other biological components, such as cellulose and fungal spores showed a small but significant contribution in winter (respectively 0.06 μg m^{-3} and $2 \cdot 10^1$ spores·m^{-3} detected on the 31st of January 2013 PM_{10} filter sample). However, the overall correlation of single $monosaccharides_{BIO}$ with each other and with other PBOA components was relatively poor, indicating a high variability in the molecular composition of the carbohydrates. Such variability highlighted the diversity of biological processes producing these sugars, clearly hindering their use as single tracers for reliably estimating PBOA concentrations in our conditions.

By ascribing all the $monosaccharides_{BIO,COARSE}$ to WSPBOA we estimated a contribution of $monosaccharides_{BIO}$ to WSPBOA of $15\%_{avg}$. Consistently, the WSPBOA average mass spectrum (Figure 1d), similarly to BBOA, showed a typical fingerprint deriving from carbohydrate fragmentation[15] as evidenced by strong contributions from $C_2H_4O_2^+$, $C_2H_5O_2^+$ and $C_3H_5O_2^+$ fragments (Figure 1b, S3, S4, S10). We estimated that >89% of the remaining WSPBOA fraction could be related to water soluble polysaccharides (after the subtraction of the $monosaccharides_{BIO}$ mass spectrum using D-mannitol and D-glucose as surrogates). This

337 estimate was based on the non-monosaccharides$_{BIO}$-WSPBOA mass spectrum, assuming
338 $C_2H_4O_2^+$, $C_2H_5O_2^+$ and $C_3H_5O_2^+$ as specific carbohydrates fragmentation tracers[15] (Figure S4),
339 and using amylopectin and starch (Figure S10) as surrogates for polysaccharides. This result,
340 together with the high cellulose contribution to OM_{COARSE}, indicated that the majority of PBOA
341 consisted of carbohydrates.

342 Part of the remaining WSPBOA fraction instead was attributed to N_{org}. 3D-PMF results
343 showed that WSPBOA explained great part of the variability of minor N-containing fragments
344 ($C_3H_9N^+$, $C_3H_8N^+$, $C_5H_{12}N^+$), consistent with XPS observations of an increased N_{org} signal in
345 PM_{COARSE}. The WSPBOA spectrum as expected showed a higher N/C ratio (0.061) than other
346 factors. Overall both the carbohydrate signature and the increased N/C content were consistent
347 with the interpretation of our factor as WSPBOA.

348 *Quantification of OM related to particulate abrasion products from leaf surfaces (OM_{PAPLS})*
349 *using n-alkanes.* *n*-alkanes (C18-C39) measured via gas chromatography mass spectrometry
350 (IDTD-GC-MS) showed distinct signatures during the different seasons and particle sizes. While
351 during winter most of the alkane mass was contained within PM_1 (90% for alkanes with an odd
352 number of C; 97% for alkanes with an even number of C), during summer only 50%$_{avg}$ and
353 70%$_{avg}$ of the odd and even alkanes were contained within PM_1. The summer-time signatures
354 were consistent with Rogge's[54] observations of alkane emissions from OM_{PAPLS} dominated by
355 odd alkanes with the highest contributions from hentriacontane (C31) followed by nonacosane
356 (C29) and tritriacontane (C33) (Figure S9). By contrast, in winter we observed a higher
357 contribution of smaller alkanes (C19-C24), without a clear odd/even predominance pattern,
358 which was consistent with winter urban observations[55] possibly related to temperature-driven
359 partitioning of combustion emissions, and consistent with vehicular fuel combustion profiles.[47,56]

This was corroborated by a slight increase in the average HOA concentration during winter compared to summer (Figure 2). We estimated the contribution of OM_{PAPLS} by applying a chemical mass balance approach (SI) using the *n*-alkanes/OM_{PAPLS} ratios reported by Rogge.[56,57] Assuming either green or dead leaves, and a possible $(OM/OC)_{green,dead\ leaves}$ range between 1.2 and 2.2, the total estimated range for $OM_{PAPLS,COARSE}$ spanned from 0.5 to 1 μg m^{-3}_{avg}, corresponding to 16-32%$_{avg}$ of the OM_{COARSE}. This result, together with high cellulose contributions, indicated that plant debris was the dominating source of OM_{COARSE}.

Fungal spores. Fungal spores measured by qPCR represented a minor component of OM. During summer, their contribution was above the detection limit only in the coarse fraction, representing just 0.01%$_{avg}$ of the OM_{COARSE} mass (corresponding to 0.4 ng m^{-3}, or $2{\cdot}10^2$ spores·m^{-3}). Nevertheless, the measured fungal spore/m^3 concentration during summer was consistent with ranges reported in other studies.[58] During winter, only one PM_{10} sample showed concentrations above the detection limits. The summer arabitol/fungal spore ($5{\cdot}10^2$ pg/spore$_{avg}$) and mannitol/fungal spore ($8{\cdot}10^2$ pg/spore$_{avg}$) ratios were noticeably variable and higher than those reported by Bauer[19] (1.2 pg arabitol/fungal spore, 1.7 pg mannitol/fungal spore), suggesting that these compounds are not unique fungal spore tracers, but given the high levels of cellulose and OM_{PAPLS} could be related to plant debris, as already proposed by other studies.[20]

Bacteria. Likewise, total bacterial mass estimated by qPCR represented a minor contributor to OM_{COARSE}. Assuming dry or wet *E. coli* cellular weights (SI), the total PM_{10} bacterial mass during summer was estimated as 1.3±0.7 ng m^{-3}_{avg} or 4±0.2 ng m^{-3}_{avg}, corresponding to $2{\cdot}10^3$ cells m^{-3}_{avg}. This is consistent with the ranges reported in other studies,[58-60] especially considering that low concentrations are commonly observed at remote and rural locations.[61] The bacterial size fractionation seasonality was similar to the other biological components: while

383 $69\%_{avg}$ of the bacterial mass was comprised between the PM_{10} and PM_1 fraction during summer,
384 all bacterial mass ($2 \cdot 10^3$ cells m^{-3}_{avg}) was detected in the submicron fraction during winter.

385 *Surface chemical composition from XPS analysis.* Another approach to look at the entire
386 aerosol is to study the chemical composition of its surface. This was performed by XPS
387 measurements, which enabled monitoring the evolution of the C_{1s} and N_{1s} BE throughout the
388 different size fractions and thus providing chemical information also about the water insoluble
389 fraction. Although XPS sensitivity was limited to the particle surface (7 nm thickness) and low
390 volatility compounds (XPS technique operates under high vacuum at 10^{-10} torr), results showed a
391 significant increase of N_{org} in the PM_{COARSE}. We resolved both an inorganic and organic N_{1s}
392 peak, with $N_{1s,org}$ occurring at a lower BE (397.7±0.3 eV, Figure 3a) than that of $N_{1s(NH_4)_2SO_4}$
393 and $NaNO_3$ (400.0±0.8 eV and 407.7±0.4 eV respectively). Likewise, tested N_{org} surrogates
394 (horseradish peroxidase and chloroperoxidase from *caldariomyces fumago*) showed the N_{1s} peak
395 occurring at similar BE (398.7±0.3 eV) corroborating our interpretation of the N_{org} peak position.
396 Overall we observed a substantial increase of the N_{org} signal in PM_{10} in comparison to PM_1
397 (Figure 3a) reflected by an N_{org}/C_{1s} ratio increase from 0.022±0.001 in PM_1 to 0.027±0.005 in
398 PM_{10}. From the N_{org}/C_{1s} ratio and from the bulk total C measurements $(TC=EC+OC)_{Sunset}$, we
399 estimated the $N_{org,1}$ and $N_{org,10}$ concentrations to be 0.05±0.03 μg m^{-3}_{avg} and 0.13±0.01 μg m^{-3}_{avg}
400 respectively. This estimate assumed N_{org} to follow the TC intra-particle concentration gradient.
401 While a crude assumption, this is the best and only methodology providing an estimate of the
402 N_{org} total mass.

403 Figure 3b displays the C_{1s} peak fitting for a PM_1 and a PM_{10} filter sample. We report an
404 increase of the less oxidized C_{1s} fraction (C_{1s} peak at lower BE) in PM_{10}, which was qualitatively
405 consistent with the odd-alkanes size fractionation. Overall, in all size fractions, the dominant C_{1s}

406 contribution did not derive from the most oxidized C_{1s} peak (Figure 3b), but from the
407 intermediate oxidized C peak, which could be related to alcohols, ketones, and aldehydes. This
408 result, although relative only to the surface and to the less volatile fractions, seemed in
409 agreement with other studies.[62]

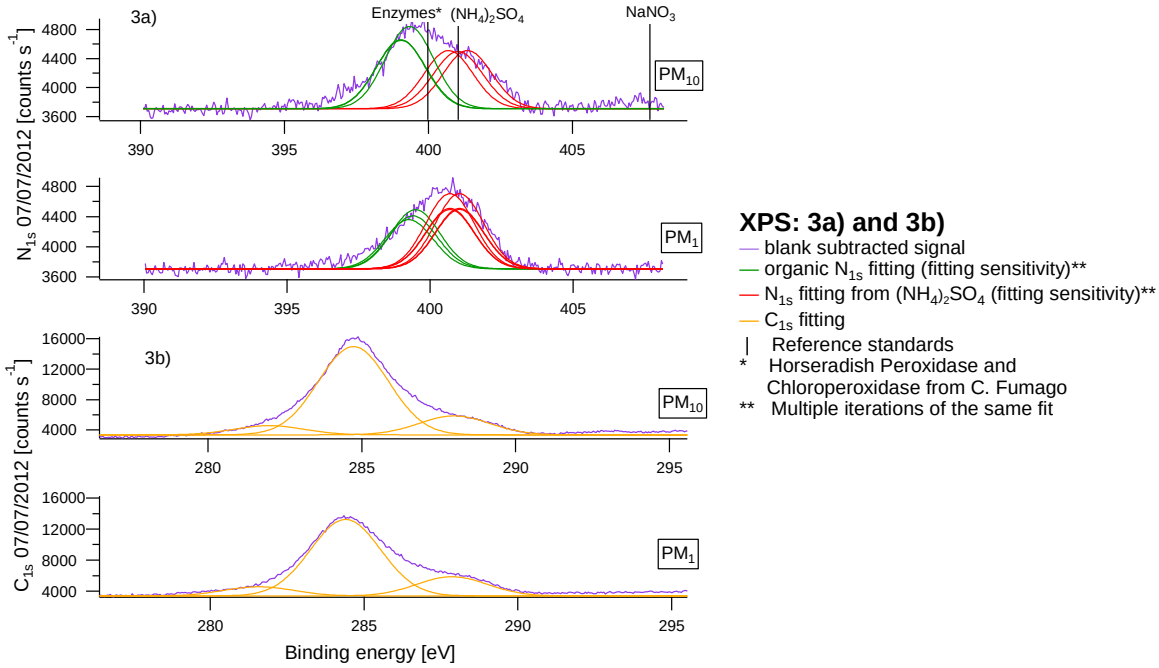

410

411 **Figure 3.** 3a) XPS measurements: N_{1s} peak fitting (PM_1 and PM_{10} sample from 04/07/2012). 3b)
412 XPS measurements: C_{1s} peak fitting (PM_1 and PM_{10} sample from 04/07/2012).

413

414 ## Yearly estimate of PBOA relative contribution to OM_{10}

415 From 3D-PMF analysis we identified a set of AMS fragments as potential PBOA tracers (figure
416 S4). Among these fragments we selected $C_2H_4O_2^+$ and $C_2H_5O_2^+$ to estimate the PBOA
417 contribution for the entire year 2013 (batch B) given their relatively high signal to noise, and
418 because they are commonly fitted in HR analysis. Both fragments showed a contribution
419 statistically higher than 0 within 1σ only to the BBOA, PBOA, and HOA factors. However,
420 given the low HOA concentration at the rural site (Figure 2a), and given the low contribution of

421 the two fragments to the HOA profile (0.02% and 0.03% respectively) we neglected the HOA
422 contribution to $C_2H_4O_2^+$ and $C_2H_5O_2^+$. Therefore the water soluble $C_2H_5O_2^+$ and $C_2H_4O_2^+$
423 fractional contribution to WSOM ($WSf\mathrm{C_2H_5O_2^+}_i$ and $WSf\mathrm{C_2H_4O_2^+}_i$) could be expressed as:

424 $$WSf\mathrm{C_2H_5O_2^+}_i = f\mathrm{C_2H_5O_2^+}_{\mathrm{WSPBOA}} \cdot \frac{WSPBOA}{WSOM}_i + f\mathrm{C_2H_5O_2^+}_{\mathrm{WSBBOA}} \cdot \frac{WSBBOA}{WSOM}_i \quad (6)$$

425 $$WSf\mathrm{C_2H_4O_2^+}_i = f\mathrm{C_2H_4O_2^+}_{\mathrm{WSPBOA}} \cdot \frac{WSPBOA}{WSOM}_i + f\mathrm{C_2H_4O_2^+}_{\mathrm{WSBBOA}} \cdot \frac{WSBBOA}{WSOM}_i \quad (7)$$

426 Where $f\mathrm{C_2H_5O_2^+}_{\mathrm{PBOA}}$, $f\mathrm{C_2H_4O_2^+}_{\mathrm{PBOA}}$, $f\mathrm{C_2H_5O_2^+}_{\mathrm{BBOA}}$, $f\mathrm{C_2H_4O_2^+}_{\mathrm{BBOA}}$ denote the $C_2H_5O_2^+$, and
427 $C_2H_4O_2^+$ fractional contributions to the WSPBOA and WSBBOA mass spectra.
428 $(\mathrm{WSPBOA/WSOM})_i$ values could be derived by solving the two linear equation system. This
429 approach will be referred to as "60/61 methodology" in the following. We assessed the accuracy
430 of the 60/61 methodology by comparing the $(\mathrm{WSPBOA/WSOM})_i$ values obtained from 3D-PMF
431 with the values predicted from the 60/61 methodology for the Batch A PM_{10} filter samples.
432 During summer the $(\mathrm{WSPBOA/WSOM})_{\mathrm{med,3D\text{-}PMF}}/(\mathrm{WSPBOA/WSOM})_{\mathrm{med,60/61\ methodology}}$ ratio was
433 0.98, while during winter 0.85. The winter discrepancy was likely due to non-negligible
434 contributions of W-OOA or other sources to $fC_2H_4O_2^+$ and $fC_2H_5O_2^+$. However the two
435 methodologies yielded highly correlated time series (R^2=0.81) and agreed within 15%, with
436 much better agreement during summer.
437 From the 60/61 methodology we estimated a WSPBOA/WSOM of $20\%_{\mathrm{avg}}$ in summer, and $6\%_{\mathrm{avg}}$
438 in winter. Assuming a R_{PBOA} of 0.18_{med} (SI), the average PBOA contribution to OM_{10} was
439 estimated as $37\%_{\mathrm{avg}}$, with higher values during summer ($60\%_{\mathrm{avg}}$ vs. $19\%_{\mathrm{avg}}$ in winter).

440 Overall, these results revealed that the contribution of PBOA to OM_{10}, mainly from plant debris,
441 may be as high as SOA contribution during summer in Payerne. While Payerne can be
442 considered as representative of typical European rural environments[50] and therefore results here
443 may be extended to other sites, other field observations are indeed required. This work represents

444 a benchmark for future field studies providing a methodology for the thorough determination of
445 PBOA mass and origin, and one of the first size-segregated datasets necessary to constrain
446 PBOA in global models.

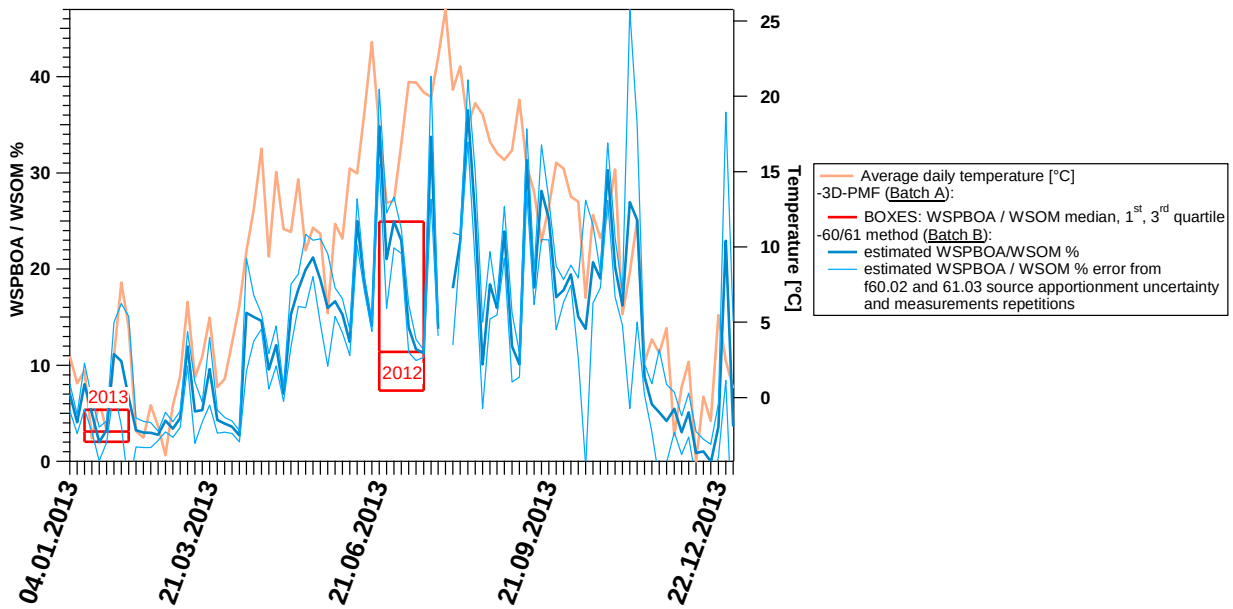

447
448
449 **Figure 4.** 2013 yearly $WSPBOA_{10}$ relative contribution to $WSOM_{10}$ estimated from the 60/61
450 methodology (Batch B). Red boxes denote WSPBOA relative contribution (median, 1st and 3rd
451 quartiles) to $WSOM_{10}$ during June-July 2012 and January-February 2013 determined by 3D-
452 PMF analysis (Batch A). The uncertainty relative to measurements repetitions and to the
453 apportionment of $fC_2H_4O_2^+$ and $fC_2H_5O_2^+$ can be interpreted as a precision estimate, while the
454 sensitivity analysis comparing 3D-PMF and 60/61 methodology results, shows an underestimate
455 of the WSPBOA/WSOM ratio calculated with the 60/61 methodology of 2% during summer and
456 15% during winter.
457

458 ASSOCIATED CONTENT

459 Supporting Information. Detailed methodology descriptions of WSOC, qPCR, XPS, and
460 IDTD-GC-ToF-MS measurements; OM_{PAPLS} determination; source apportionment optimization.
461 This material is available free of charge via the Internet at http://pubs.acs.org.

AUTHOR INFORMATION

Corresponding Author

*Address: OFLA/004, 5232 Villigen PSI, Switzerland; Phone: +41 56 310 4202; e-mail: andre.prevot@psi.ch.

*Address: OFLB/002, 5232 Villigen PSI, Switzerland; Phone: +41 56 310 2785; e-mail: imad.el-haddad@psi.ch.

Author Contributions

[†]C.B. wrote the manuscript. [†]C.B. and [†*]I.E.H performed the data analysis and source apportionment. [†*]A.S.H.P., [†*]I.E.H., [†]C.B. and [†]J.G.S. designed the experiment. [†]C.B. and [†]A.K. performed the offline-AMS analysis. [≠]P.F. and [≠]R.G. performed WSOC measurements. [ᵣ]J.S. measured carbohydrates$_{meas}$ and EC/OC. [‡]C.H. collected the samples, and measured ions and EC/OC. [¯]G.A., [¯,◊]R.Z., and [¯]J.S.-K. performed IDTD-GC-ToF-MS measurements. [•]Y.R., T.S.M. and [•]Y.M. performed qPCR measurements. [¤]M.E.K., C.B. and I.E.H. performed XPS measurements. [ð]A.K.-G. and [ð]M.F. performed cellulose measurements. All authors gave approval to the final version of the manuscript.

Funding Sources

This work was supported by the Federal Office for the Environment in Switzerland

ACKNOWLEDGMENT

Carlo Bozzetti acknowledges the Lithuanian–Swiss Cooperation Programme “Research and Development” project AEROLIT (Nr. CH-3-.MM-01/08). Imad El Haddad acknowledges the Swiss National Science Foundation (project number IZERZ0 142146). Yinon Rudich

483 acknowledges support from the Israel Science Foundation, grant #913/12 and from the Dollond
484 Foundation. We acknowledge Saurer, M. and Schmid, L. for providing milled oak leaves, and
485 Goldsmith G. R. for the NCBI BLAST research.

486 REFERENCES

487 (1) Pasteur, L. Mémoire sur les corpuscles organises qui existent dans l'atmosphere. Examen
488 de la doctrine des générations spontanées. Ann. Sci. Nat. Zool. **1861**, 16, 5–98.

489 (2) Carnelly, T.; Haldane, J. S.; Anderson, A. M. The carbon acid, organic matter, and micro-
490 organisms in air, more especially of dwellings and schools. Philos. Transact. R. Soc. Lond.
491 B. **1887**, 178, 61–111.

492 (3) Fuzzi, S.; Baltensperger, U.; Carslaw, K.; Decesari, S.; Denier van der Gon, H.; Facchini,
493 M. C.; Fowler, D.; Koren, I.; Langford, B.; Lohmann, U.; Nemitz, E.; Pandis, S.; Riipinen,
494 I.; Rudich, Y.; Schaap, M.; Slowik, J. G.; Spracklen, D. V.; Vignati, E.; Wild,
495 M.; Williams, M.; Gilardoni. S. Particulate matter, air quality and climate: lessons learned
496 and future needs. Atmos. Chem. Phys. **2015**, 15, 8217-8299.

497 (4) Després, V. R.; Huffman, J. A.; Burrows, S. M; Hoose, C.; Safatov, A. S.; Buryak, G.;
498 Fröhlich-Nowoisky, J.; Elbert, W.; Andreae, M. O.; Pöschl, U.; Jaenicke, R. Primary
499 biological aerosol particles in the atmosphere: a review. Tellus B. **2012**, 64, 15598.

500 (5) Douwes, J.; Thorne, P.; Pearce, N.; Heederik, D. Bioaerosol health effects and exposure
501 assessment: progress and prospects. Ann. Occup. Hyg. **2003**, 47, 187–200.

(6) Hiranuma, N.; Möhler, O.; Yamashita, K.; Tajiri, T.; Saito, A.; Kiselev, A.; Hoffmann, N.; Hoose, C.; Jantsch, E.; Koop, T.; Murakami M. Ice nucleation by cellulose and its potential contribution to ice formation in clouds. Nature Geosci. **2015**, 8, 273-277.

(7) Hader, J. D.; Wright, T. P.; Petters. M. D. Contribution of pollen to atmospheric ice nuclei concentrations Atmos. Chem. Phys. **2014**, 14, 5433-5449.

(8) Gurian-Sherman, D.; Lindow., S. E.; Bacterial ice nucleation: significance and molecular basis. FASEB J. **1993**,14, 1338-1343.

(9) Andreae, M. O.; Rosenfeld, D. Aerosol-cloud-precipitation interactions. Part 1. The nature and sources of cloud-active aerosols. Earth Sci. Rev. **2008**, 89, 13–41.

(10) Ariya, P. A.; Sun, J., Eltouny, N. A.; Hudson, E. D.; Hayes, C. T; Kos, G. Physical and chemical characterization of bioaerosols–implications for nucleation processes. Int. Rev. Phys. Chem. **2009**, 28, 1–32.

(11) Andreae, M. O. Aerosols before pollution. Science. **2007**, 315, 50-51.

(12) Fu, P.; Kawamura, K.; Chen, J.; Qin, M.; Ren., L.; Sun, Y.; Wang, Z.; Barrie, L. A.; Tachibana, E.; Ding, A.; Yamashita, Y. Fluorescent water-soluble organic aerosol in the High Arctic atmosphere. Sci. Rep. **2015**, 5, 9845.

(13) Pöhlker, C.; Huffman, J. A.; Pöschl U. Autofluorescence of atmospheric bioaerosols - fluorescent biomolecules and potential interferences. Atmos. Meas. Tech., **2012**, 5, 37–71.

(14) Chen, Q.; Farmer, D. K.; Schneider, J.; Zorn, S. R.; Heald, C. L; Karl, T. G.; Guenther, A.; Allan, J. D.; Robinson, N.; Coe, H.; Kimmel, J. R.; Pauliquevis, T.; Borrmann, S.; Pöschl, U.; Andreae, M. O.; Artaxo, P.; Jimenez, J. L.; Martin, S. T. Mass spectral

characterization of submicron biogenic organic particles in the Amazon Basin. Geophys. Res. Lett. **2009**, 36, L20806.

(15) Schneider, J.; Freutel, F.; Zorn, S. R.; Chen, Q.; Farmer, D. K.; J. L. Jimenez, Martin, S. T. Artaxo, P.; Wiedensohler, A.; Borrmann, S. Mass-spectrometric identification of primary biological particle markers: indication for low abundance of primary biological material in the pristine submicron aerosol of Amazonia. Atmos. Chem. Phys. Discuss. **2011**, 11, 19143–19178.

(16) Pöschl, U., Martin, S. T., Sinha, B., Chen, Q., Gunthe, S. S.; Huffman, J. A.; Borrmann, S.; Farmer, D.K.; Garland, R. M.; Helas, G.; Jimenez, J. L.; King, S. M.; Manzi, A.; Mikhailov, E.; Pauliquevis, T.; Petters, M. D.; Prenni, A. J.; Roldin, P.; Rose, D.; Schneider, J.; Su, H.; Zorn, S. R.; Artaxo, P.; Andreae, M. O. Rainforest aerosols as biogenic nuclei of clouds and precipitation in the Amazon. Science. **2010**, 329, 1513–1516.

(17) IPCC, 2013: Climate Change 2013: The Physical Science Basis. Contribution of Working Group I to the Fifth Assessment Report of the Intergovernmental Panel on Climate Change [Stocker, T.F.; Qin, D.; Plattner, G.-K.; Tignor, M.; Allen, S. K.; Boschung, J.; Nauels, A.; Xia, Y.; Bex, V.; Midgley, P. M. (eds.)]. Cambridge University Press, Cambridge, United Kingdom and New York, NY, USA, 1535 pp.

(18) Heald, C. L.; Spracklen D. V. Atmospheric budget of primary biological aerosol particles from fungal spores. Geophys. Res. Lett. **2009**, 36, L09806-L09806.

(19) Bauer, H.; Claeys, M.; Vermeylen, R.; Schueller, E.; Weinke, G.; Berger, A.; Puxbaum, H. Arabitol and mannitol as tracers for the quantification of airborne fungal spores, Atmos. Environ. **2008**, 42, 588–593.

545 (20) Burshtein, N.; Lang-Yona, N.; Rudich, Y. Ergosterol, arabitol and mannitol as tracers for
546 biogenic aerosols in the eastern Mediterranean. Atmos. Chem. Phys. **2011**, 11, 829–839.

547 (21) Daellenbach, K. R.; Bozzetti, C.; Krepelova, A.; Canonaco, F.; Huang, R.-J.; Wolf, R.;
548 Zotter, P.; Crippa, M.; Slowik, J.; Zhang, Y.; Szidat, S.; Baltensperger, U.; Prévôt, A. S.
549 H.; El Haddad, I. Characterization and source apportionment of organic aerosol using
550 offline aerosol mass spectrometry. Atmos. Meas. Tech. **2016**, 9, 23-29.

551 (22) Birch, M. E.; Cary, R. A. Elemental carbon-based method for monitoring occupational
552 exposures to particulate diesel exhaust. Aerosol Sci. and Tech. **1996**, 25, 221–241.

553 (23) Cavalli, F.; Viana, M.; Yttri, K. E.; Genberg, J.; Putaud, J. P. Toward a standardised
554 thermal-optical protocol for measuring atmospheric organic and elemental carbon: the
555 EUSAAR protocol. Atmos. Meas. Tech. **2010**, 3, 79-89.

556 (24) Piazzalunga, A.; Bernardoni, V.; Fermo, P.; Vecchi, R.Optimisation of analytical
557 procedures for the quantification of ionic and carbonaceous fractions in the atmospheric
558 aerosol and applications to ambient samples.Anal Bioanal Chem. **2013**, 405, 1123-32.

559 (25) Kunit, M.; Puxbaum, H. Enzymatic determination of the cellulose content of atmospheric
560 aerosols. Atmos. Environ. **1996**, 30, 1233-1236.

561 (26) Orasche, J.; Schnelle-Kreis, J.; Abbaszade, G.; Zimmermann, R. Technical Note: In-situ
562 derivatization thermal desorption GC-TOFMS for direct analysis of particle-bound non-
563 polar and polar organic species. Atmos. Chem. Phys. **2011**, 11, 8977-8993.

564 (27) Lang-Yona, N.; Dannemiller, K.; Yamamoto, N.; Burshtein, N.; Peccia, J.; Yarden, O.;
565 Rudich, Y. Annual distribution of allergenic fungal spores in atmospheric particulate

matter in the Eastern Mediterranean; a comparative study between ergosterol and quantitative PCR analysis. Atmos. Chem. Phys. **2012**, 12, 2681–2690.

(28) Lang-Yona, N.; Lehahn, Y.; Herut, B.; Burshtein, N.; Rudich, Y. Marine aerosol as a possible source for endotoxins in coastal areas. Sci. Total Environ. **2014**, 499, 311–318.

(29) Yttri, K. E.; Schnelle-Kreis, J.; Maenhaut, W.; Abbaszade, G.; Alves, C.; Bjerke, A.; Bonnier, N.; Bossi, R.; Claeys, M.; Dye, C.; Evtyugina, M.; García-Gacio, D.; Hillamo, R.; Hoffer, A.; Hyder, M.; Iinuma, Y.; Jaffrezo, J.-L.; Kasper-Giebl, A.; Kiss, G.; López-Mahia, P. L.; Pio, C.; Piot, C.; Ramirez-Santa-Cruz, C.; Sciare, J.; Teinilä, K.; Vermeylen, R.; Vicente, A.; Zimmermann, R. An intercomparison study of analytical methods used for quantification of levoglucosan in ambient aerosol filter samples, Atmos. Meas. Tech., **2015**, 8, 125-147.

(30) DeCarlo, P. F.; Kimmel, J. R.; Trimborn, A.; Northway, M. J.; Jayne, J. T.; Aiken, A. C.; Gonin, M.; Fuhrer, K.; Horvath, T.; Docherty, K. S.; Worsnop, D. R.; Jimenez, J. L. Field-deployable, high-resolution, time-of-flight aerosol mass spectrometer. Anal. Chem. **2006**, 78, 8281–8289.

(31) Hospodsky, D.; Yamamoto, N.; Peccia, J.; Accuracy, precision, and method detection limits of quantitative PCR for airborne bacteria and fungi. Appl. Environ. Microb. **2010**, 76, 7004-7012.

(32) Sundararaj, S.; Guo, A.; Habibi-Nazhad, B.; Rouani, M.; Stothard, P.; Ellison, M.; Wishart, D. S. The CyberCell Database (CCDB): a comprehensive, self-updating, relational database to coordinate and facilitate in silico modeling of Escherichia coli. Nuclei Acid Res. **2004**, 32, D263-D265.

(33) Crilley, L. R.; Ayoko, G. A.; Morawska, L. Analysis of organic aerosols collected on filters by Aerosol Mass Spectrometry for source identification. Anal. Chim. Acta. **2013**, 803, 91– 96.

(34) Paatero, P.; Tapper, U. Positive matrix factorization - a nonnegative factor model with optimal utilization of error-estimates of data values. Environmetrics **1994**, 5, 111-126.

(35) Ulbrich, I. M.; Canagaratna, M. R.; Cubison, M. J.; Zhang, Q.; Ng, N. L.; Aiken, A. C.; Jimenez, J. L. Three-dimensional factorization of size-resolved organic aerosol mass spectra from Mexico City. Atmos. Meas. Tech. **2012**, 5, 195–224.

(36) Tucker, L. R. Some mathematical notes on 3-mode factor analysis. Psychometrika **1966**, 31, 279–311.

(37) Paatero, P.; Hopke, K. Rotational tools for factor analytic models. J. Chemometr. **2009**, 23, 91–100.

(38) Canonaco, F.; Crippa, M.; Slowik, J. G.; Baltensperger, U.; Prévôt, A. S. H. SoFi, an IGOR-based interface for the efficient use of the generalized multilinear engine (ME-2) for the source apportionment: ME-2 application to aerosol mass spectrometer data. Atmos. Meas. Tech. **2013**, 6, 3649-3661.

(39) Mohr, C.; DeCarlo, P. F.; Heringa, M. F.; Chirico, R.; Slowik, J. G.; Richter, R.; Reche, C.; Alastuey, A.; Querol, X.; Seco, R.; Penuelas, J.; Jimenez, J. L.; Crippa, M.; Zimmermann, R.; Baltensperger, U.; Prevot, A. S. H. Identification and quantification of organic aerosol from cooking and other sources in Barcelona using aerosol mass spectrometer data. Atmos. Chem. Phys. **2012**, 12, 1649-1665.

609 (40) Aiken, A. C.; DeCarlo, P. F.; Kroll, J. H.; Worsnop, D. R.; Huffmann, J. A.; Docherty, K.
610 S.; Ulbrich, I. M.; Mohr, C.; Kimmel, J. R.; Sueper, D.; Sun, Y.; Zhang, Q.; Trimborn, A.;
611 Northway, M.; Ziemann, P. J.; Canagaratna, M. R.; Onasch, T. B.; Alfarra, M. R.; Prevot,
612 A. S. H.; Dommen, J.; Duplissy, J.; Metzger, A.; Baltensperger, U.; Jimenez J. L. O/C and
613 OM/OC ratios of primary, secondary, and ambient organic aerosols with high-resolution
614 time-of-flight aerosol mass spectrometry. Environ. Sci. Technol., **2008**, 42, 4478-4485.

615 (41) Allan, J. D.; Jimenez, J. L.; Williams, P. I.; Alfarra, M. R.; Bower, K. N.; Jayne, J. T.;
616 Coe, H.; Worsnop, D. R. Quantitative sampling using an Aerodyne aerosol mass
617 spectrometer 1. Techniques of data interpretation and error analysis. J. Geophys. Res.,
618 **2003**, 108 (D3), 4090.

619 (42) Ulbrich, I. M.; Canagaratna, M. R.; Zhang, Q.; Worsnop, D. R.; Jimenez, J. L.
620 Interpretation of organic components from positive matrix factorization of aerosol mass
621 spectrometric data. Atmos. Chem. Phys. **2009**, 9, 2891-2918.

622 (43) Crippa, M.; Canonaco, F.; Slowik, J. G.; El Haddad, I.; DeCarlo, P. F.; Mohr, C.;
623 Heringa, M. F.; Chirico, R.; Marchand, N.; Temime-Roussel, B.; Abidi, E.; Poulain,
624 L.; Wiedensohler, A.; Baltensperger, U.; Prévôt; A. S. H. Primary and secondary organic
625 aerosol origin by combined gas-particle phase source apportionment. Atmos. Chem. Phys.
626 **2013**, 13, 8411-8426.

627 (44) Barmpadimos, I.; Nufer, M.; Oderbolz, D. C.; Keller, J.; Aksoyoglu, S.; Hueglin, C.;
628 Baltensperger, U.; Prevot A. S. H. The weekly cycle of ambient concentrations and traffic
629 emissions of coarse (PM(10)-PM(2.5)) atmospheric particles, Atmos. Environ. **2011**, 45,
630 4580-4590.

631 (45) Chow, J.; Watson, J.; Ashbaugh, L. L.; Magliano, K. L. Similarities and differences in
632 PM10 chemical source profiles for geological dust from the San Joaquin Valley, California.
633 Atmos. Environ. **2003**, 37, 1317-1340.

634 (46) Amato, F.; Pandolfi, M; Moreno, T.; Furger, M.; Pey, J.; Alastuey, A.; Bukowiecki, N.;
635 Prevot, A.S.H.; Baltensperger, U.; Querol X. Sources and variability of inhalable road dust
636 particles in three European cities. Atmos. Environ. **2011**, 45, 6777-6787.

637 (47) El Haddad, I.; Marchand, N.; Drona, J.; Temime-Roussel, B.; Quivet, E.; Wortham, H.;
638 Jaffrezo, J.-L.; Baduel, C.; Voisin, D.; Besombes, J. L.; Gille, G. Comprehensive primary
639 particulate organic characterization of vehicular exhaust emissions in France. Atmos.
640 Environ. **2009**, 43, 6190-6198.

641 (48) Huang, R.-J.; Zhang, Y.; Bozzetti, C.; Ho, K.-F.; Cao, J.; Han, Y.; Dällenbach, K. R.;
642 Slowik, J. G.; Platt, S. M.; Canonaco, F.; Zotter, P.; Wolf, R.; Pieber, S. M.; Bruns, E. A.;
643 Crippa, M.; Ciarelli, G.; Piazzalunga, A.; Schwikowski, M.; Abbaszade, G.; Schnelle-
644 Kreis, J.; Zimmermann, R.; An, Z.; Szidat, S.; Baltensperger, U.; El Haddad, I.; Prévôt, A.
645 S. H. High secondary aerosol contribution to particulate pollution during haze events in
646 China, Nature. **2014**, 514, 218-212.

647 (49) Canonaco, F.; Slowik, J. G.; Baltensperger, U.; Prévôt, A. S. H. Seasonal differences in
648 oxygenated organic aerosol composition: implications for emissions sources and factor
649 analysis. Atmos. Chem. Phys. **2015**, 15, 6993-7002.

650 (50) Crippa, M.; Canonaco, F.; Lanz, V. A.; Äijälä, M.; Allan, J. D.; Carbone, S.; Capes, G.;
651 Ceburnis, D.; Dall'Osto, M.; Day, D. A.; DeCarlo, P. F.; Ehn, M.; Eriksson, A.; Freney, E.;
652 Hildebrandt Ruiz, L.; Hillamo, R.; Jimenez, J. L.; Junninen, H.; Kiendler-Scharr, A.;

Kortelainen, A.- M.; Kulmala, M.; Laaksonen, A.; Mensah, A. A.; Mohr, C.; Nemitz, E.; O'Dowd, C.; Ovadnevaite, J.; Pandis, S. N.; Petäjä, T.; Poulain, L.; Saarikoski, S.; Sellegri, K.; Swietlicki, E.; Tiitta, P.; Worsnop, D. R.; Baltensperger, U.; Prévôt, A. S. H. Organic aerosol components derived from 25 AMS data sets across Europe using a consistent ME-2 based source apportionment approach. Atmos. Chem. Phys. **2014**, 14, 6159–6176.

(51) Medeiros, P. M.; Conte, M. H.; Weber, J. C.; Simoneit, B. R. T. Sugars as source indicators of biogenic organic carbon in aerosols collected above the Howland Experimental Forest, Maine. Atmos. Environ. **2006**, 40, 1694-1705.

(52) Jia, Y.; Clements, A. L.; Fraser, M. P. Saccharide composition in atmospheric particulate matter in the southwest US and estimates of source contributions. J. Aerosol Sci. **2010**, 41, 62-73.

(53) Williams, L. R.; Gonzalez, L. A.; Peck, J.; Trimborn, D.; McInnis, J.; Farrar, M. R.; Moore, K. D.; Jayne, J. T.; Robinson, W. A.; Lewis, D. K.; Onasch, T. B.; Canagaratna, M. R.; Trimborn, A.; Timko, M. T.; Magoon, G.; Deng, R.; Tang, D.; de la Rosa Blanco, E.; Prévôt, A. S. H.; Smith, K. A.; Worsnop D. Characterization of an aerodynamic lens for transmitting particles greater than 1 micrometer in diameter into the Aerodyne aerosol mass spectrometer. Atmos. Meas. Tech. **2013**, 6, 3271–3280.

(54) Rogge, W. F.; Hildemann, L. M.; Mazurek, M. A.; Cass, G. R; Simoneit, B. R. T. Sources of fine organic aerosol. 4. Particulate abrasion products from leaf surfaces of urban plants, *Environ. Sci. Technol.*, **1993**, *27* (13), 2700–2711.

673 (55) Kotianová, P.; Puxbaum, H.; Bauer, H.; Caseiro, A.; Marrb, I. L.; Čìk, G.; Temporal
674 patterns of n-alkanes at traffic exposed and suburban sites in Vienna. Atmos. Environ.
675 **2008**, 42, 2993–3005.

676 (56) Rogge, W. F.; Hildemann, L. M.; Mazurek, M.,A.; Caw, G. R. Sources of Fine Organic
677 Aerosol. 2. Noncatalyst and Catalyst-Equipped Automobiles and Heavy-Duty Diesel
678 Trucks. Environ. Sci. Technol. **1993**, 27, 636-651.

679 (57) Hildemann, L. M.; Mazurek, M. A.; Cass, G. R.; Simoneit, B. R. Quantitative
680 characterization of urban sources of organic aerosol by high-resolution gas-
681 chromatography, Environ. Sci. Technol. **1991**, 25, 1311-1325.

682 (58) Borodulin, A.; Safatov, A.; Belan, B.; Panchenko, M. Measurement errors in determining
683 tropospheric bioaerosol concentrations in the southern region of Western Siberia. Dokl.
684 Biol. Sci. **2005**, 403, 260–262.

685 (59) Vlodavets, V.; Mats, L. The influence of meteorological factors on the microflora of the
686 atmospheric air in Moscow. J. Microbiol. **1958**, 59, 539–544.

687 (60) Pady, S.; Kelly, C. Aerobiological studies of fungi and bacteria over the Atlantic Ocean.
688 Can. J. Botany. **1954**, 32, 202–212.

689 (61) Burrows, S. M.; Elbert, W.; Lawrence, M. G.; Pöschl, U. Bacteria in the global
690 atmosphere–Part 1: Review and synthesis of literature data for different ecosystems.
691 Atmos. Chem. Phys. **2009**, 9, 9281–9297.

692 (62) El Haddad, I.; D'Anna, B.; Temime-Roussel, B.; Nicolas, M.; Boreave, A.; Favez, O.;
693 Voisin, D.; Sciare, J.; George, C.; Jaffrezo, J.-L. ; Wortham, H.; Marchand, N.

694 Towards a better understanding of the origins, chemical composition and aging of
695 oxygenated organic aerosols: case study of a Mediterranean industrialized environment,
696 Marseille. Atmos. Chem. Phys. **2013**, 13, 7875-7894.

697

698

699 Graphical TOC Entry

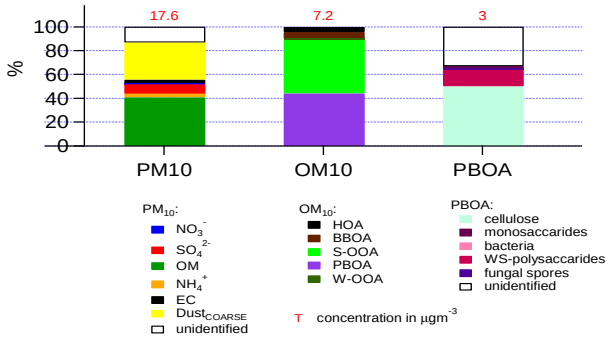

700